The following publication Z. Zhou, W. Lin and Y. -X. Sun, "Wideband Circularly Polarized High-Efficiency Rectenna With Large-Angle Wireless Power Capture Capability," in IEEE Antennas and Wireless Propagation Letters, vol. 23, no. 12, pp. 4428-4432, Dec. 2024 is available at https://doi.org/10.1109/LAWP.2024.3450310.

Wideband Circularly-Polarized High-Efficiency Rectenna with Large-Angle Wireless Power Capture Capability

Zengtai Zhou, Wei Lin, *Senior Member, IEEE*, and Yu-Xiang Sun, *Member, IEEE*

***Abstract*—This letter proposes a wideband high-efficiency circularly-polarized (CP) semi-transparent rectenna with large-angle wireless power capture capability. It consists of a wideband and broadbeam CP receiving antenna and a highly efficient rectifier. The wideband and broadbeam CP characteristics are achieved by combining a grounded stub with a coplanar waveguide (CPW) slot antenna. The antenna is meshed and fabricated on a glass substrate to realize a certain degree of optical transparency (OT). For the rectifier, a fan-stub impedance matching network is designed to broaden the impedance bandwidth and improve the AC to DC conversion efficiency. The measured results show that the receiving antenna achieves a wide usable CP bandwidth of 21.55% (2.07-2.57 GHz). Broad measured CP beams of 125° and 119° in the two planes are also obtained at 2.45 GHz. When the receiving antenna is cascaded with the high-efficiency rectifier, the proposed rectenna realizes a wide over-60%-efficiency bandwidth of 21.55% (2.07-2.57 GHz) with a peak efficiency of 72.47% at an input power of 10 dBm, showing great potential for wireless energy harvesting (WEH) and wireless power transfer (WPT) applications.**

***Index Terms*—Broadbeam antenna, circular polarization, high efficiency rectenna, wireless energy harvesting, wireless power transfer.**

I. INTRODUCTION

Wireless energy harvesting (WEH) and wireless power transfer (WPT) technologies have become the key battery-free options in smart cities due to their sustainability and environmental-friendly [1, 2]. An essential component of WEH technology is a rectenna, which consists of a receiving antenna and a rectifier circuit. The rectenna can harvest electromagnetic energy and convert it into DC power.

The receiving antenna in a rectenna can be linearly polarized or circularly polarized (CP). The latter one is usually preferred due to its avoidance to multipath interference and the ability to receive electromagnetic waves of different polarizations [3]–[5]. As shown in Fig. 1(a), with broad beams and wide bandwidth, the receiving antenna attached on window glass achieves a larger spatial and spectrum coverage for capturing both indoor and outdoor electromagnetic energies [6].

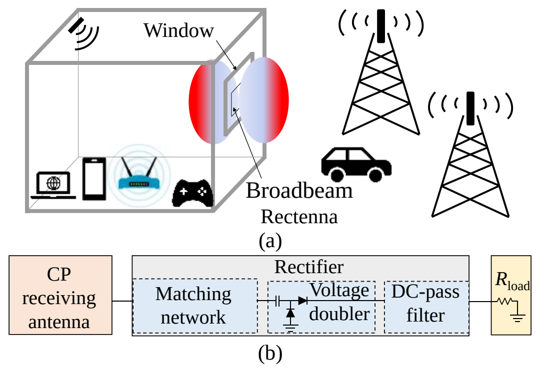

Fig. 1. (a) Application scenario of the broadbeam rectenna on window glass of a building. (b) Block diagram of the proposed rectenna.

In recent years, transparent antennas have attracted much attention for their ability to transmit and receive wireless signals without affecting the visual effect. Conventional transparent antennas using water and other transparent liquids [7, 8] may not be suitable for antenna miniaturization and integration. An alternative is a low-profile metal mesh structure on transparent substrates, including wideband dual-polarized antenna [9] and polarization converting CP antenna on PET [10], and metal mesh patch antenna on acrylic [11]. Transparent antennas on glass substrate are another low-cost approach and they can be integrated into window glass of buildings, display screens of electronic devices, and windshields of vehicles [12]-[16], for wireless communication and WEH [17, 18].

The rectifier circuit is another critical component of rectennas and has a significant impact on the conversion efficiency and operating bandwidth. Several techniques have been introduced to increase the efficiency and bandwidth, such as harmonic termination networks [19] and different impedance matching networks using capacitors [20], stubs [21]-[25] or combinations of stubs with inductors [26] and LC tanks [27].

Manuscript received 2024. This work was supported in part by the National Natural Science Foundation of China under grants U23A20288 and 62001306, and in part by Shenzhen Science and Technology Program under grants KQTD20221101093555005, ZDSYS20220527171402005, and 20231122102327003, and in by the Research Grants Council of the Hong Kong SAR, China, under Projects PolyU 25213623 and AoE/E-101/23-N. (*Corresponding author: Yu-Xiang Sun*).

Zengtai Zhou and Yu-Xiang Sun are with the State Key Laboratory of Radio Frequency Heterogeneous Integration (Shenzhen University), and with College of Electronics and Information Engineering, Shenzhen University, Shenzhen 518060, China. Yu-Xiang Sun is also with Shenzhen Institute of Artificial Intelligence and Robotics for Society (AIRS), Shenzhen, China (e-mail: eeyxsun@szu.edu.cn).

Wei Lin is with the Photonics Research Institute, Department of Electrical and Electronic Engineering, The Hong Kong Polytechnic University, Hong Kong, SAR, China (e-mail: w.lin@polyu.edu.hk).

Color versions of one or more of the figures in this article are available online at http://ieeexplore.ieee.org.

These methods can achieve either a wide usable bandwidth or a high peak efficiency. However, the in-band efficiency is unstable, limiting their practical applications.

This letter presents a high-efficiency semi-transparent rectenna with wideband and broadbeam circular polarization for large-angle wireless power capture. The receiving antenna incorporates a coplanar waveguide (CPW) T-shaped structure with a grounded stub to realize wideband circular polarization with broad beams. To obtain high OT, the CPW slot antenna features a meshed design and is fabricated on a glass substrate. The rectifier employs a fan-stub impedance matching network to realize high efficiency across a wide operating bandwidth. Measured results show that the proposed rectenna achieves a wide angular coverage of over 119 °, a wide usable CP and over-60%-efficiency overlapping bandwidth of 21.55% (2.07-2.57 GHz) with a peak efficiency of 72.47%.

II. Rectenna Design

Fig. 1(b) shows the block diagram of the proposed rectenna. It consists of a wideband and broadbeam CP receiving antenna with high OT and a highly efficient rectifier, which includes an impedance matching network, a voltage doubler based on two diodes, and a DC-pass filter.

A. Receiving Antenna

A wideband and broadbeam CP semi-transparent CPW slot antenna is used as the receiving antenna in the rectenna. The geometry of the receiving antenna is shown in Fig. 2. A glass substrate with a thickness of h and a dielectric constant of ε_r is used. It has a length of l_1 and a width of w_1. Since the antenna is only printed on one side of the glass substrate, the ungrounded CPW feeding method is employed. The widths of the center signal line and the gap are w and g, respectively. To generate CP radiation, a T-shaped feeding strip and a rectangular stub are placed within the slot area. The rectangular stub, with a width of w_3 and a length of l_3, is connected to the left side of the ring ground at a distance of g_0 from the horizontal part of the T-shaped strip. In order to obtain OT, a mesh structure is deployed for the whole antenna. It is noted that the transparency can be improved by increasing the uncovered area of the mesh unit, however, this would reduce the antenna efficiency [15]. As a compromise, the slot length and the line width of the mesh unit are chosen as g_1 and g_2, respectively.

Fig. 3 shows the simulated surface current distributions of the receiving antenna, and right-handed circular polarization (RHCP) radiation is generated in the boresight (+z-axis) direction. Due to the symmetry of the antenna, left-handed CP radiation can be also obtained by mirroring the rectangular stub with respect to the *xoz* plane.

The coupling between the rectangular stub and the T-shaped strip affects the current distribution and the CP performance. The effects of the distance g_0 between the rectangular stub and the T-shaped strip on the reflection coefficient and axial ratio (AR) of the antenna are shown in Fig. 4. It can be seen that good impedance matching and a wide 3-dB AR bandwidth can be obtained with a proper g_0 of 0.3 mm. However, the AR performance deteriorates when g_0 becomes too small (0.05 mm) or too large (0.6 mm) due to the tight or loose coupling.

The design of the antenna can therefore start with the initial sizes of the T-shaped strip and the ring ground, which determine the operating band. The distance g_0 is then adjusted to obtain a wide 3-dB AR bandwidth. It is noted that the above design and optimization process can be performed based on the solid metal structure, which can be transformed into a meshed transparent structure without affecting the antenna performance by selecting appropriate mesh size parameters g_1 and g_2 [16].

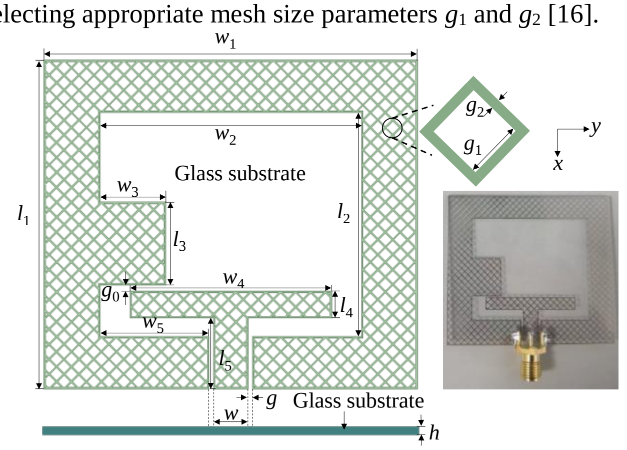

Fig. 2. Geometry and prototype of the CP transparent receiving antenna. The dimensions are: l_1 = 44 mm, l_2 = 30 mm, l_3 = 11.1 mm, l_4 = 3.6 mm, l_5 = 10 mm, w_1 = 50 mm, w_2 = 35 mm, w_3 = 8.8 mm, w_4 = 27 mm, w_5 = 14.6 mm, w = 5.8 mm, g_0 = 0.3 mm, g_1 = 1.2 mm, g_2 = 0.2 mm, g = 0.6 mm, h = 1 mm.

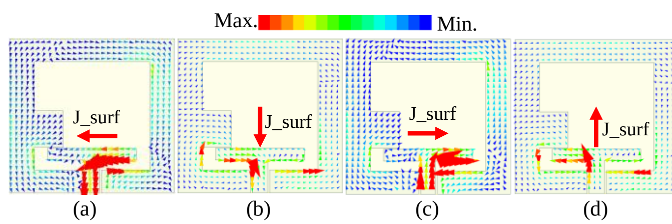

Fig. 3. Surface current distributions of the CP transparent receiving antenna at 2.45 GHz. (a) t = 0 °, (b) t = 90 °, (c) t = 180 °, (d) t = 270 °.

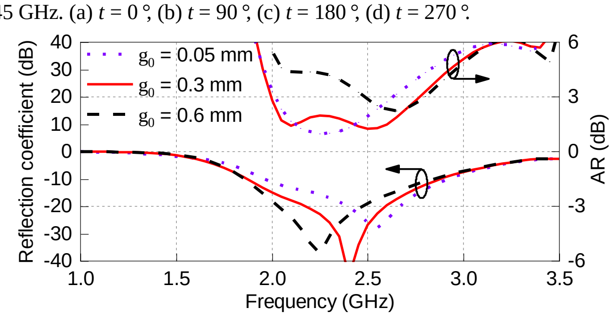

Fig. 4. The effect of g_0 on the reflection coefficient and boresight AR of the receiving antenna.

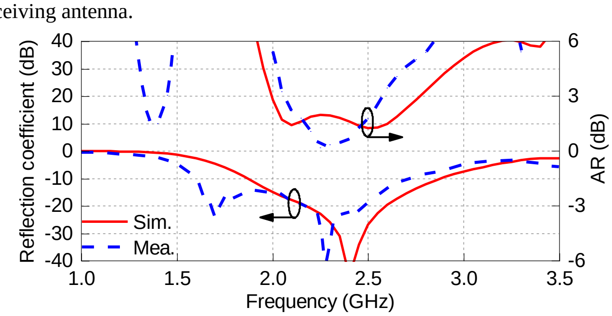

Fig. 5. Simulated and measured reflection coefficient and boresight AR of the CP transparent receiving antenna.

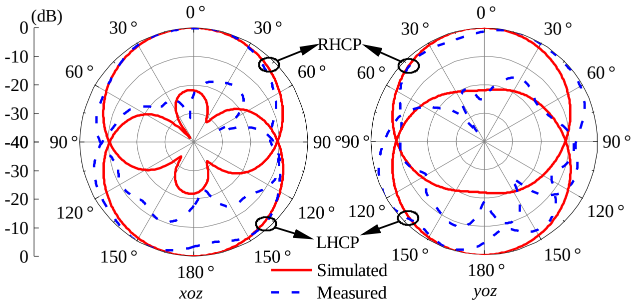

Fig. 6. Measured and simulated radiation patterns of the broadbeam CP transparent receiving antenna at 2.45 GHz.

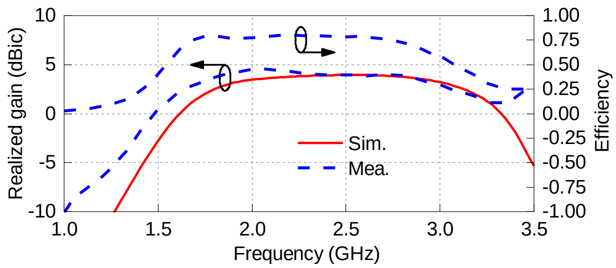

Fig. 7. Measured and simulated boresight realized gain and measured antenna efficiency.

The CP transparent receiving antenna was fabricated and measured. The simulated and measured reflection coefficients of the antenna are shown in Fig. 5 and good impedance matching can be observed. The measured results show a -10-dB impedance bandwidth of 51.85% (1.60–2.72 GHz) and are shifted to the left compared to the simulated results of 42.19% (1.87–2.87 GHz). The ARs of the transparent antenna are also shown in Fig. 5 and reasonable agreement is found. The measured and simulated 3-dB AR bandwidths are 21.55% (2.07–2.57 GHz) and 33.76% (1.97–2.77 GHz), respectively. The discrepancy between the simulation and measurement is mainly due to the processing tolerance. It should be noted that wide usable CP bandwidth of this antenna, *i.e*. the overlapping part between -10-dB impedance and 3-dB AR bandwidths, is obtained as 21.55% (2.07–2.57 GHz).

The measured and simulated radiation patterns of the CP receiving antenna at 2.45 GHz are shown in Fig. 6. In the boresight (+z-axis) direction, the difference between the front RHCP and back LHCP is greater than 22 dB, indicating high purity of RHCP radiation. Broad measured 3-dB AR beams of 125° and 119° are obtained in the *xoz* and *yoz* planes, respectively, showing wide angular coverage. Due to the CP features in both boresight and back directions, the antenna can receive signals from two directions. Fig. 7 shows the simulated and measured boresight realized gain. The measured in-band gains vary in the range of 2.07–4.55 dBi. Fig. 7 also shows the measured antenna efficiency, which is stable at around 80% in the operating band.

The OT of the meshed antenna is calculated as 73.47%, which is the fraction of the uncovered transparent area over the total area. It is also measured as 72.95% by using a Linshang LS108A lens transmission meter.

B. Rectifier Design

In this design, a wideband rectifier with high in-band efficiency is proposed by using a fan-stub impedance matching network.

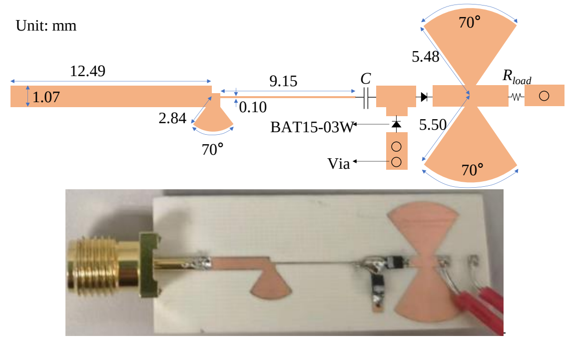

Fig. 8. Layout and prototype of the wideband high-efficiency rectifier.

The layout and prototype of the proposed rectifier are shown in Fig. 8. A substrate with a dielectric constant of 3.66, a thickness of 0.508 mm, and a loss tangent of 0.0037 is used for the fabrication. To adapt to the low input power environment and generate a high output voltage, two BAT15-03W Schottky diodes with low turn-on voltage are used for the voltage doubler. Two fan-shaped parallel stubs are inserted at the output of the voltage doubler to work as a DC-pass filter, which has a wider filtering band compared to quarter-wavelength open-ended transmission lines [25], allowing more energy to be reflected to the diodes for rectification. A narrow inductive transmission line is cascaded before the voltage doubler to cancel its capacitance. To adjust the operating frequency and further reduce the fluctuation of the impedance of the rectifier, another fan-shaped stub is connected in parallel between the narrow inductive transmission line and the input 50 Ω transmission line. After optimization in Keysight ADS, the dimensions of the rectifier are finalized and shown in Fig. 8. In addition, to achieve high conversion efficiency, the DC blocking capacitor *C* and the output load resistance are optimized to 10 pF and 950 Ω, respectively.

The simulated and measured reflection coefficients of the rectifier at different input powers P_{in} are shown in Fig. 9. The -10-dB impedance bandwidths at different input powers are almost the same, but with different matching levels. At an input power of 10 dBm, the measured -10 dB bandwidth is 28.70% (1.97–2.63 GHz). Fig. 9 also shows the simulated and measured conversion efficiencies. It can be seen that the efficiency curves are very close to each other at the input powers of 10 dBm and 12 dBm. The input power of 10 dBm is chosen, with a measured peak efficiency of 73.14%.

With an input power of 10 dBm, the efficiencies of the rectifier with different output loads R_L are shown in Fig. 10. In the range of 600–2000 Ω, the efficiencies are around 60% within the frequency band of 2.05–2.61 GHz. Optimum efficiency is achieved with an output load of 950 Ω.

Taking into account both the -10 dB impedance matching and the 60% conversion efficiency, the operating bandwidth of the rectifier is 27.19% (1.97-2.59 GHz). When the CP receiving antenna and the rectifier are cascaded as a rectenna, an overlapping bandwidth of 21.55% (2.07-2.57 GHz) between the

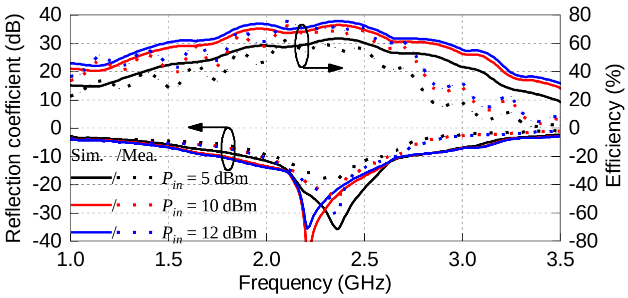

Fig. 9. Simulated and measured reflection coefficient and conversion efficiency of the rectifier at different input powers P_{in}.

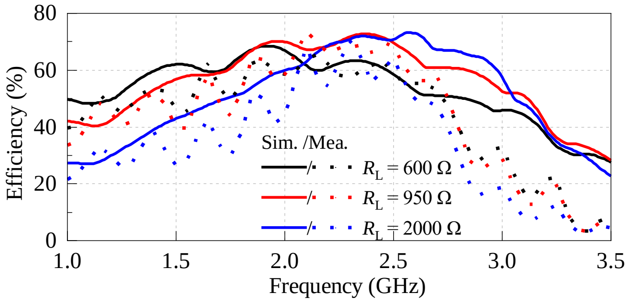

Fig. 10. Simulated and measured conversion efficiencies of the rectifier at an input power of 10 dBm with different output load R_L.

usable CP bandwidth of the antenna and the 60%-efficiency bandwidth of the rectifier is obtained.

III. Measurement And Discussion of Rectenna

In this section, the proposed rectenna is measured and its measurement setup is shown in Fig. 11. In the measurement, the RF signal from the Ceyear 1435B signal generator is amplified by an LNA and transmitted through a standard gain horn antenna. A multimeter is used to measure the DC voltage V_{out} of the output load R_{load} of the rectenna. The conversion efficiency can be expressed as

$$\eta = \frac{P_{out}}{P_{in}} = \frac{V_{out}^2}{P_{in} \times R_{load}} \quad (1)$$

where the input power P_{in} is measured by a Keysight FieldFox N9914A spectrum analyzer. Before measuring the rectenna, the receiving antenna is connected to the spectrum analyzer to ensure that the power received at a distance d at the measuring frequency is 10 dBm. In the measurement of the rectifier in the previous section, it is directly connected to the signal generator for a certain input power P_{in}.

Fig. 12 shows the efficiency comparison between the rectenna and the rectifier. The measured peak efficiency of the rectenna is 72.47% at 2.1 GHz which is lower than the 73.14% of the rectifier. Over the frequency range from 2 GHz to 2.6 GHz, the in-band efficiency of the rectenna is slightly lower than that of the rectifier, which is due to the unstable power received from the air interface by the receiving antenna compared to that coming directly from the connected signal generator and the mismatch between the receiving antenna and the rectifier.

Table I compares the proposed rectenna with some previous rectenna designs. It can be seen that most designs are linearly

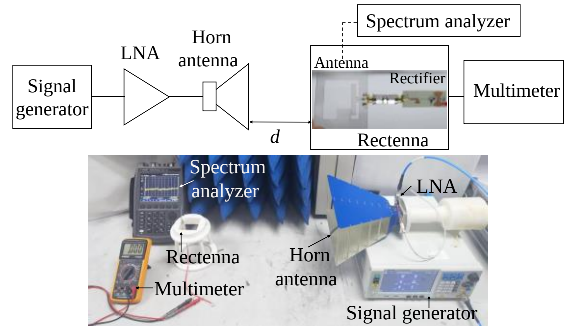

Fig. 11. Diagram and photograph of the measurement setup.

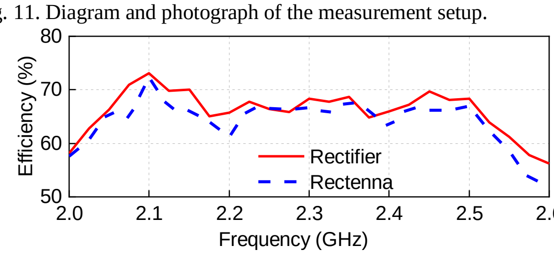

Fig. 12. Measured conversion efficiency of the proposed rectenna and rectifier at an input power P_{in} of 10 dBm.

polarized, which would suffer from polarization mismatch. Although [19] and [26] can realize CP characteristics, their usable bandwidths are within 10%. In terms of the operating bandwidth with over 60% efficiency, our rectenna is only second to the LP design of [5]. Rectennas in [17] and [18] are optically transparent, but with low efficiency. Our design, with a high OT of 72.95%, can achieve broadband usable CP bandwidth of 21.55%, wide over-60%-efficiency operating bandwidth of 24.83%, and high peak efficiency of 72.47%, which is beneficial for many WEH scenarios.

TABLE I
COMPARISON BETWEEN OUR DESIGNS AND SOME RELATED WORKS

Rectennas	Rectenna (Rx antenna+Rectifier)			Rx antenna
	Peak Eff.	Input Power	>60%-eff. BW	Usable CP BW
[2]	72.5%	13 dBm	14.43%	LP
[5]	68%	10 dBm	26.6%	LP
[17]	50%	-6 dBm	N.A.	LP
[18]	26%	-10 dBm	N.A.	LP
[19]	74.2%	10 dBm	3.98%	RHCP, 9.8%
[26]	51.1%	0.5 dBm	N.A.	RHCP, 3.57%
This work	72.47%	10 dBm	24.83%	RHCP, 21.55%

Rx antenna: receiving antenna. BW: bandwidth. LP: linearly polarized.

IV. Conclusion

In this letter, a high-efficiency wideband and broadbeam CP semi-transparent rectenna is developed. The measured results show that the receiving antenna achieves an OT of 72.95% and broad 3-dB AR beams of larger than 119°. When the receiving antenna is cascaded with the rectifier, the proposed rectenna achieves both wide usable CP operation and 60% conversion efficiency with an overlapping bandwidth of 21.55% (2.07-2.57 GHz). A peak efficiency of 72.47% is also achieved.

References

[1] H. J. Visser and R. J. M. Vullers, “RF energy harvesting and transport for wireless sensor network applications: Principles and requirements,” *Proc. IEEE*, vol. 101, no. 6, pp. 1410–1423, Jun. 2013.

[2] M. -J. Nie, X. -X. Yang, G. -N. Tan, and B. Han, “A compact 2.45-GHz broadband rectenna using grounded coplanar waveguide,” *IEEE Antennas Wireless Propag. Lett.*, vol. 14, pp. 986-989, Dec. 2015.

[3] Y. Liu, K. Huang, Y. Yang, and B. Zhang, “A low-profile lightweight circularly polarized rectenna array based on coplanar waveguide,” *IEEE Antennas Wireless Propag. Lett.*, vol. 17, no. 9, pp. 1659-1663, Sept. 2018.

[4] J. Sang, L. Qian, M. Li, J. Wang, and Z. Zhu, “A wideband and high-gain circularly polarized antenna array for radio-frequency energy harvesting applications,” *IEEE Trans. Antennas Propag.*, vol. 71, no. 6, pp. 4874-4887, June 2023.

[5] S. F. Bo, J. -H. Ou, Y. Dong, S. -W. Dong, and X. Y. Zhang, “All-polarized wideband rectenna with enhanced efficiency within wide input power and load ranges,” *IEEE Trans. Ind. Electron.*, vol. 69, no. 7, pp. 7470-7480, Jul. 2022.

[6] Y.-X. Sun, K. W. Leung and K. Lu, “Broadbeam cross-dipole antenna for GPS applications,” *IEEE Trans. Antennas Propag.*, vol. 65, no. 10, pp. 5605–5610, Oct. 2017

[7] J. Li et al., “A fan-shaped compact water antenna with wide bandwidth and optical transparence,” *IEEE Trans. Antennas Propag.*, vol. 70, no. 4, pp. 3017-3021, Apr. 2022.

[8] J. Sun and K.-M. Luk, “A wideband low cost and optically transparent water patch antenna with omnidirectional conical beam radiation patterns,” *IEEE Trans. Antennas Propag.*, vol. 65, no. 9, pp. 4478–4485, Sep. 2017.

[9] C. Ding, L. Liu, and K.-M. Luk, “An optically transparent dual polarized stacked patch antenna with metal-mesh films,” *IEEE Antennas Wireless Propag. Lett.*, vol. 18, no. 10, pp. 1981–1985, Oct. 2019.

[10] T. Liu et al., “A broadband circularly polarized antenna based on transparent conformal metasurface,” *IEEE Antennas Wireless Propag. Lett.*, vol. 22, no. 12, pp. 3197-3201, Dec. 2023.

[11] S. H. Kang and C. W. Jung, “Transparent patch antenna using metal mesh,” *IEEE Trans. Antennas Propag.*, vol. 66, no. 4, pp. 2095-2100, April 2018.

[12] S. Abirami B., E. F. Sundaesingh, and Harshavardhini A., “A compact conformal windshield antenna for location tracking on vehicular platforms,” *IEEE Trans. Veh. Technol.*, vol. 68, no. 4, pp. 4047–4050, Apr. 2019.

[13] W. Hong, S. Lim, S. Ko, and Y. G. Kim, “Optically invisible antenna integrated within an OLED touch display panel for IoT applications,” *IEEE Trans. Antennas Propag.,* vol. 65, no. 7, pp. 3750–3755, Jul. 2017.

[14] P. D. Tung and C. W. Jung, “Optically transparent wideband dipole and patch external antennas using metal mesh for UHD TV applications,” *IEEE Trans. Antennas Propag.,* vol. 68, no. 3, pp. 1907–1917, Mar. 2020.

[15] Y.-X. Sun, D. Wu, X. Fang, and J. Ren, “On-glass grid structure and its application in highly-transparent wideband antenna for internet of vehicles,” *IEEE Trans. Veh. Technol.*, vol. 72, no. 1, pp. 93–101, Jan. 2023.

[16] W. Zhong and Y.-X. Sun, “Wideband circularly polarized antenna on glass substrate with high optical transparency,” *Int. Symp. Antennas Propag. (ISAP)*, Sydney, Australia, Oct. 31–Nov. 3, 2022.

[17] S. Bellal, H. Takhedmit, and L. Cirio, “Design and experiments of transparent rectennas for wireless power harvesting,” *IEEE Wireless Power Transfer Conf. (WPTC)*, Aveiro, Portugal, 2016, pp. 1-4.

[18] H. Takhedmit, L. Cirio, F. Costa, and O. Picon, “Transparent rectenna and rectenna array for RF energy harvesting at 2.45 GHz,” *European Conf. Antennas Propag. (EuCAP)*, The Hague, Netherlands, 2014, pp. 2970-2972.

[19] C. Cao, X. Zhang, C. Song, A. Georgiadis, and G. Goussetis, “A highly integrated multipolarization wideband rectenna for simultaneous wireless information and power transfer (SWIPT),” *IEEE Trans. Antennas Propag.*, vol. 71, no. 10, pp. 7980-7991, Oct. 2023.

[20] W. Lin and R. W. Ziolkowski, “Electrically small single-substrate Huygens dipole rectenna for ultracompact wireless power transfer applications,” *IEEE Trans. Antennas Propag*., vol. 69, no. 2, pp. 1130-1134, Feb. 2021.

[21] Y. Shi, Y. Fan, Y. Li, L. Yang, and M. Wang, “An efficient broadband slotted rectenna for wireless power transfer at LTE band,” *IEEE Trans. Antennas Propag.*, vol. 67, no. 2, pp. 814-822, Feb. 2019.

[22] Y. Yang et al., “A circularly polarized rectenna array based on substrate integrated waveguide structure with harmonic suppression,” *IEEE Antennas Wireless Propag. Lett*., vol. 17, no. 4, pp. 684-688, Apr. 2018.

[23] L. Guo, H. Fang, X. Li, W. Yang, and K. Wu, “A rectenna design with quasi-full spatial coverage based on a compact dielectric resonator antenna,” *IEEE Trans. Antennas Propag.*, vol. 71, no. 10, pp. 7870-7880, Oct. 2023.

[24] L. Guo, X. Li, W. Sun, W. Yang, Y. Zhao, and K. Wu, “Designing and modeling of a dual-band rectenna with compact dielectric resonator antenna,” *IEEE Antennas Wireless Propag. Lett*., vol. 21, no. 5, pp. 1046-1050, May 2022.

[25] X. -X. Yang, C. Jiang, A. Z. Elsherbeni, F. Yang, and Y. -Q. Wang, “A novel compact printed rectenna for data communication systems,” *IEEE Trans. Antennas Propag.*, vol. 61, no. 5, pp. 2532-2539, May 2013.

[26] P. Lu, C. Song, and K. M. Huang, “A two-port multipolarization rectenna with orthogonal hybrid coupler for simultaneous wireless information and power transfer (SWIPT),” *IEEE Trans. Antennas Propag.*, vol. 68, no. 10, pp. 6893-6905, Oct. 2020.

[27] P. Lu, C. Song, and K. M. Huang, “Ultra-wideband rectenna using complementary resonant structure for microwave power transmission and energy harvesting,” *IEEE Trans. Microw. Theory Techn.*, vol. 69, no. 7, pp. 3452-3462, Jul. 2021.